Uppermost mantle velocity from Pn tomography in the Gulf of Aden

Jordane Corbeau, Frédérique Rolandone, Sylvie Leroy, A. Al-Lazki, A.L. Stork, Derek Keir, G.W. Stuart, J.O.S. Hammond, Cécile Doubre, J. Vergne, et al.

Uppermost mantle velocity from Pn tomography in the Gulf of Aden

Jordane Corbeau[1,2], F. Rolandone[1,2], S. Leroy[1,2], A. Al-Lazki[3,4], A. L. Stork[5], D. Keir[6], G. W. Stuart[7], J. O. S. Hammond[8], C. Doubre[9], J. Vergne[9], A. Ahmed[1,10] and K. Khanbari[11]

[1] Sorbonne Universités, UPMC Univ Paris 06, UMR 7193, Institut des Sciences de la Terre Paris (iSTeP), F-75005 Paris, France (jordane.corbeau@upmc.fr; frederique.rolandone@upmc.fr; sylvie.leroy@upmc.fr).

[2] CNRS, UMR 7193, Institut des Sciences de la Terre Paris (iSTeP), F-75005 Paris, France

[3]Department Earth Sciences, Sultan Qaboos University, PO Box 36, Postal Code 123, Alkhod, Muscat, Sultanate of Oman (lazki@squ.edm.om).

[4]Exploration Department, Petroleum Development Oman, PO Box 81, Postal Code 100, Mina Al-Fahal, Sultanate of Oman

[5] School of Earth Sciences, University of Bristol, Bristol BS8 1RJ, UK (anna.stork@bristol.ac.uk).

[6] National Oceanography Center Southampton, University of Southampton, Southampton, SO14 3ZH, UK (D.Keir@soton.ac.uk).

[7] Institute of Geophysics and Tectonics, School of Earth and Environment, University of Leeds, Leeds, LS2 9JT, UK (g.w.stuart@leeds.ac.uk).

[8] Faculty of Engineering, Department of Earth Science and Engineering, Imperial College of London, London, SW7 2AZ, UK (j.hammond@imperial.ac.uk).

[9] EOST, IPGS, Univ. Strasbourg, France (cecile.doubre@unistra.fr; jerome.vergne@unistra.fr).

[10] Seismological and Volcanological Observatory Center, Dhamar, Yemen (hakim66@myself.com).

[11]Sana'a University, Yemen Remote Sensing and GIS Center, Yemen (kkhanbari@hotmail.com).

ABSTRACT

We determine the lateral variations in seismic velocity of the lithospheric mantle beneath the Gulf of Aden and its margins by inversion of Pn travel times. Data for this study was collected by several temporary seismic networks and from the global catalogue. A least-squares tomographic

algorithm is used to solve for velocity variations in the mantle lithosphere. In order to separate shallow and deeper structures, we use separate inversions for shorter and longer ray path data. High Pn velocities (8.2 to 8.4 km/s) are observed in the uppermost mantle beneath Yemen that may be related to the presence of magmatic underplating of the volcanic margins of Aden and Red Sea. Zones of low velocity (7.7 km/s) are present in the shallow upper mantle beneath Sana'a, Aden, Afar, and along the Gulf of Aden that are likely related to melt transport through the lithosphere feeding active volcanism. Deeper within the upper mantle, beneath the Oman margin, a low velocity zone (7.8 km/s) suggests a deep zone of melt accumulation. Our results provide evidence that the asthenosphere undergoes channelized flow from the Afar hotspot towards the east along the Aden and Sheba Ridges.

INTRODUCTION

The Afar triple junction separates the Arabian Plate from the African Plate. This triple junction is characterized by abundant magmatic activity due to the presence of elevated temperatures associated with the Afar mantle plume, suggested to have played an important role in the continental break-up that led to the opening of the Red Sea and the Gulf of Aden rifts (Bellahsen et al., 2003). Deformation within the region is largely localized along these two rifts (Leroy et al., 2010). Seismic imaging studies carried out in this region have led to a better understanding of the lithospheric structure and the role played by the Afar plume in the volcanic activity and continental break-up. Shear wave velocity variations studied by Park et al. (2008) indicate the presence of low velocity regions at depths greater than 150 km beneath the Red Sea coast and the volcanic structures in Saudi Arabia. These velocity anomalies may be the result of hot material from the Afar plume flowing north beneath Arabia and along the Red Sea rift (e.g. Chang and Van der Lee, 2011). Continental margins in the western Gulf of Aden are volcanic while eastern margins are non-volcanic. The gravity study of Hébert et al. (2001) suggests the influence of the Afar plume is limited to the western part of the gulf. They found that the oceanic crustal thicknesses obtained from

inversion of mantle Bouguer anomaly east of 45°E are typical of a normal crust generated outside any hot spot influence. However, several subsequent studies have pointed out the presence of low velocity anomalies associated with partial melting in Oman (Basuyau et al., 2010), off-axis volcanism near the Sheba ridge (d'Acremont et al., 2010) and magmatic activity within the mantle beneath the entire Gulf of Aden (e.g. compilation of several investigations: electromagnetism, geochemistry, heat flow, see for a review Leroy et al., 2010). On the basis of geophysical measurements and teleseismic body-wave tomography, Leroy et al. (2010) and Chang and Van der Lee (2011) suggested that hot mantle material from the Afar plume may be flowing eastward along the inverted channel at the base of the lithosphere created by the Gulf of Aden ridges. In order to test this hypothesis we need robust constraints on the wavespeed of the uppermost mantle, constraints which are lacking from the previous regional and global studies which could not place constraints on mantle structure above 75 km depth (Park et al., 2007; Park et al., 2008; Chang and Van der Lee, 2011; Debayle et al., 2001; Phillips et al., 2007).

Here we describe the first regional study of lithospheric mantle P-wave velocities (Pn) along the Gulf of Aden. Pn are high-frequency compressional waves that are refracted in the lithospheric mantle at about 8 km/s (Beghoul et al., 1993). Pn tomography studies can be used to interpret the rheology and the physical characteristics of the Mohorovicic discontinuity and the uppermost mantle (Bannister et al., 1991). Wave propagation velocities provide constraints on temperature, pressure, and compositional variations within the mantle (Perry et al., 2006). They are also used to study the spatial distribution of mantle upwelling and partial melting (Dunn et al., 2001). For this study we use the inversion method of Hearn (1996) to analyze Pn arrival times in data from networks of seismometers temporarily deployed in the region. Pn tomography allows us to image variations of wave propagation speed within the lithospheric mantle beneath the Gulf of Aden. These velocity variations are then interpreted within the context of regional geodynamics.

The aim of this work is to image the mantle structure of the entire Gulf of Aden and the triple

junction of the Red-Sea – Gulf of Aden – East-African rifts. In doing so, we can test models that explain the origin and distribution of volcanism along the Gulf of Aden.

DATA

The data consist of Pn first arrival times recorded by local networks deployed in Oman, Yemen and Socotra Island (Fig. 1) from April 2009 to May 2011 during the YOCMAL project: 23 stations were deployed in Oman, 60 stations arranged in 3 profiles in Yemen, and 24 stations on Socotra Island. Data collected from 2003 to 2007 by existing networks in Oman and Socotra were included in the study (Dhofar Seismic Experiment network, Fig. 1). We also used data from networks in Djibouti (2009 to 2011), Ethiopia (2007 to 2010, Afar Rift Consortium, Afar0911 and IRIS-PASSCAL networks) and Saudi Arabia (2009 to 2010, permanent station RAYN) (Fig. 1).

Pn waves are compressional head waves which travel along or below the Moho discontinuity, and are recorded at regional-scale distances (about 200 km to 1600 km). We used Pn arrival times for seismic events occurring at epicentral distances of 1.8° to 16° from each receiver, and we precisely hand-picked 13530 Pn arrival times. We combine our data with data from the ISC global catalogue in order to improve the data set and tomography model resolution (comparisons of the resolution between ISC data only and the combined data set with hand-picked Pn are provided in the Supplemental File, Figures DR1 and DR2). From the ISC catalogue we selected 65985 arrival times that are identified as Pn waves from events that occurred from 1990 to 2010 within a 2000 km diameter zone centered at 17°N, 54°E. Several selection criteria were used to improve the data set quality. Only earthquakes with depths less than 35 km were selected. Each station was required to record five or more events and each event had to be recorded by at least five stations. To minimize location errors the following criteria were used: event locations calculated with a minimum of 8 stations; azimuth gap < 200°; rms residuals < 3 s; nearest station used in the calculation < 800 km. All travel times selected were then plotted as a function of distance (Fig. 2) and only data with travel time residuals of 4 seconds or less relative to the mean mantle velocity were retained. We

found 52947 arrival times from 3778 events and 352 stations that satisfied the above criteria (Fig. 3).

The distribution of seismic stations is not evenly spread over the entire study area. There is a high density of stations along the northern coast of the Gulf of Aden and in the Afar hotspot region. There are only a few stations across the rest of the Arabian plate and no stations in Somalia. The greatest number of seismic events occurred in the Zagros mountain belt and along the Aden Ridge.

Figure 4 shows the ray path density for the selected arrival times and for the tomographic model. Regions with the highest density of Pn ray paths (> 64 rays by cell) occur near the Afar triple junction, the northern coast of Gulf of Aden and an area between the western Gulf of Aden and Socotra Island. Intrusions of dyke swarms in the Afar region have triggered seismic episodes of a large number of highly-localized, < M5 seismic events over a period of a few days or weeks (e.g. Wright et al., 2006; Ebinger et al., 2010; Grandin et al., 2011; Keir et al., 2011; Nobile et al., 2012) leading to high data density in the Afar region. At the time of the study, the most recent such swarm was located east of Djibouti, at 44°E, in November 2010 (Ahmed et al., 2013a; Shuler and Nettles, 2012; Ebinger et al., 2013). One hundred seismic events were recorded over a period of two days, principally from the Socotra Island network. This episode is one of the largest observed from an oceanic spreading centre (Shuler and Nettles, 2012; Ahmed et al., 2013a). Areas with Pn arrivals numbering between 4 and 64 predominate in the rest of the study area. Data coverage is very good in the Afar region and on the northern margin of the Gulf of Aden, where most of the stations are located. Data coverage is poorest in the southern Saudi Arabia, the easternmost part of the Gulf of Aden and the southern margin.

METHOD

The Pn data inversion method for velocity was developed and described by Hearn (1996). Pn rays are sensitive to lateral propagation velocity variations in the upper mantle, to crustal thickness variations, and to crustal propagation velocity variations (Hearn and Ni, 1994). Following the

method of Hearn (1996) our investigation focuses on the Pn velocity variations assuming an isotropic medium and a ray path divided into three straight segments: (1) the focus-mantle path, (2) the mantle path and (3) the mantle–station path, which are then adjusted for the curvature of the Earth. For the inversion, the uppermost layer of the mantle is divided into a set of two dimensional cells. The slowness (inverse of velocity) is determined for each cell by solving the Pn total travel time equation:

$$T_{ij} = a_i + b_j + \Sigma\, d_{ijk} * S_k$$

where T_{ij} is the travel time along the ray path from event j to station i, a_i is the travel time for the mantle-station path arriving at station i, b_j is the travel time for the focus-mantle path for event j, d_{ijk} is the distance traveled by ray ij in mantle cell k and S_k is the slowness perturbation (inverse of velocity) for cell k. The travel time equation is solved for each cell and for each event–station ray path using a conditional least squares (LSQR) algorithm (Paige and Saunders, 1982; Hearn, 1996) to obtain the slowness of the lithospheric mantle. An iteration number of 500 was used to reach LSQR inversion convergence. A number of analyses were performed to select optimum cell size. The best solutions of the travel time equation were obtained using a cell size of 0.25° by 0.25°. The Laplace damping equation was used during the inversion to control the smoothness of the solution. After a series of tests, we chose a damping parameter of 500. This value was found to best balance error reduction and model resolution. Damping values of less than 200 where found to produce spurious velocity anomalies, while values larger than 800 significantly reduced our model resolution. When the LSQR algorithm initialization occurs, mean mantle velocity is calculated from the slope of the linear trend line of the arrival time versus distance plot.

RESOLUTION AND ERROR ANALYSIS

The estimated standard error for the Pn inversion in the method of Hearn (1996) is typically on the order of one second, indicating the presence of weak noise that comes from event location errors (Hearn et al., 2004; Calvert et al., 2000). We find a consistent value in our model inversion of 0.87

151 seconds. Standard errors for velocity were calculated using the bootstrap method for 50 iterations
152 (Hearn and Ni, 1994). The resulting average velocity error is 0.05 km/s. Velocity errors are less than
153 0.17 km/s, much smaller than the amplitude of anomalies interpreted. Synthetic tests were used to
154 determine the resolution of the inversion model for the study area, and to quantify the ability of the
155 inversion model to distinguish small-scale features. Checkerboard test models were used with cell
156 sizes of 2° by 2° and 4° by 4° (Fig. 5) with a random Gaussian noise of 1s to simulate travel time
157 estimation errors. Input velocity anomalies alternate between +0.25 km/s and -0.25 km/s. For the 4°
158 by 4° checkerboard test (Fig. 5c), the resolution is very good on the northern margin and along the
159 Gulf of Aden. The lack of seismological stations and of seismic events on the southern Gulf of Aden
160 result in poor resolution on the southern margin, the eastern Sheba Ridge, and areas near the edge of
161 the study area. For the 2° by 2° checkerboard test, high resolution areas are located at the junction
162 of Red Sea and the Gulf of Aden and along the northern margin of the Gulf of Aden. Small-scale
163 features of about 2° by 2° can be interpreted in these areas.

164 **RESULTS**

165 **Results of inversion**

166 Figure 6 shows the result of the inversion for 500 iterations. Velocity anomalies are in km/s and are
167 relative to a mean mantle propagation velocity of 8.16 km/s, calculated by the model with our data
168 set. A prominent low velocity anomaly (7.7 km/s) is located between Socotra Island and the Omani
169 margin. Smaller low velocity anomalies are imaged in Afar (7.8 km/s), in the southern Red Sea,
170 around Sana'a (7.7 km/s) and in the western Gulf of Aden (7.8 km/s). Finally, two small high
171 velocity anomalies are observed on the western coast of Yemen and in the central Gulf of Aden (8.4
172 km/s).

173 **Variation of mantle velocity with depth**

174 Pn are first arrivals from seismic events that occur about 200 km from the receiver, so that the
175 waves travel near the crust/mantle interface. Ray paths do not travel strictly along the crust/mantle

interface but dive into the lithospheric mantle (Hearn et al., 2004). The greater the distance of the event from the station, the deeper the waves travel into the lithospheric mantle, such that short and long ray paths do not travel in the same part of the lithospheric mantle. Quantifying the precise depth of Pn ray penetration remains challenging. It is possible, however, to separate short ray paths from long ones. Short ray paths arriving from events that occur at angular distances of 1.8° to 9.5° travel through the shallow lithospheric mantle (SLM) and long ray paths from 9.5° to 16° travel through the deeper lithospheric mantle (DLM) (Hearn et al., 2004). Travel-time inversion can be performed for short and long ray paths separately. The reduced data in each inversion results in reduced model resolution. Nevertheless, the resolution is sufficient to distinguish major structures. Checkerboard tests models are used for both SLM and DLM and results are presented in Figure 7. Ray path coverage is denser in the western part of the SLM, yielding resolution of better than 2° by 2° (Fig. 7a). Resolution is 4° by 4° of greater in the eastern SLM (Fig. 7c). It is not possible to resolve features as small as 2° by 2° in the DLM (Fig. 7b), but 4° by 4° features are resolved for the eastern part (Fig. 7d). The data set for the DLM has a large number of ray paths from events located around the Zagros mountain belt. This results in some NE-SW streaking of the checkerboard.

Results of the SLM and DLM inversions are shown in Figures 7e and 7f, respectively. The mean propagation velocity of waves in the mantle is 8.09 km/s for short ray paths, corresponding to the SLM, and 8.20 km/s for long ray paths (DLM). We find a velocity gradient between the SLM and the DLM, as expected in the lithospheric mantle (Hearn et al., 2004). Figure 7e shows velocity variations of Pn-waves for the SLM. The most visible structures are low velocity anomalies in the Afar region, the southern Red Sea, around Sana'a, and along the Gulf of Aden (7.7 km/s). High velocity anomalies appear along the western and southern margins of Yemen (8.2 to 8.4 km/s). For the DLM (Fig. 7f), low velocity anomalies with high amplitude are situated in southern Oman and in the north of Socotra Island (7.8 km/s). A high velocity anomaly is located between the southern Omani margin and the Sheba Ridge. The separation of the data set into short and long ray paths

shows the different distribution of velocity anomalies in the SLM and DLM.

DISCUSSION AND GEODYNAMIC IMPLICATIONS

Upper mantle structure

Previous tomographic studies at various scales of resolution have been carried out within the Gulf of Aden. The global Pn tomography study of Phillips et al. (2007) imaged velocity anomalies with a resolution of 4° to 8°. They found that all of the Red Sea and its borders are marked by a pronounced low velocity anomaly whereas only a weak low velocity anomaly occurs in the western Gulf of Aden. In contrast, the eastern end of the gulf does not show any low velocity anomaly. Using S-wave tomography, Debayle et al. (2001) found a low velocity anomaly around Afar and Yemen, along the Red Sea, and along the Gulf of Aden. This low velocity zone was imaged at a depth of 100 km with a resolution of a few hundred kilometers. Chang and Van der Lee (2011), using S-wave teleseismic tomography, imaged a low velocity anomaly at depths of 75 and 100 km with a resolution of 1° in the western Gulf of Aden, southern Red Sea, and Afar region. In the Red Sea region, the large-scale low velocity anomaly (7.8 km/s) that we imaged within the SLM reaches the Saudi Arabian coast between latitudes 15°N and 18°N. It is situated under the eastern margin of the Red Sea. Park et al. (2008) imaged a similar anomaly using S-wave teleseismic tomography. In contrast, our Pn tomography of the margin along the coast of Oman shows a slightly higher velocity relative to the 8.1 km/s mean mantle velocity. These results are consistent with heat flow measurements in Arabia, which show that heat flow is high along the Red Sea coast in Yemen, but low near the coast of the Gulf of Aden in Oman (Rolandone et al., 2013).

When the SLM Pn tomographic map of the Gulf of Aden is superposed on a map of current magmatic and volcanic activity, low velocity anomalies correlate well with zones of active volcanism (Fig. 8). Along the southern Yemeni margin, low velocity anomalies (7.9 km/s) appear beneath active volcanic structures (stars in the map, Fig. 8). Two pronounced low velocity anomalies (7.7 km/s) are positioned under volcanic structures in the Afar region and around Sana’a

226 in Yemen. A slight low velocity anomaly (8.0 km/s) on the Omani margin is situated under a recent
227 active volcano (latitude 16°N – longitude 54°E; Fig. 8 top; Leroy et al., 2000). One low velocity
228 anomaly corresponds to recently volcanic activity on the western Aden Ridge associated with an
229 episode of magmatic dyke intrusion in November 2010 (Shuler and Nettles, 2012; Ahmed et al.,
230 2013a).
231 Broad low velocity anomalies (7.7 km/s) are imaged in the region of Socotra Island. In the north of
232 Socotra, velocity anomalies of at least 4° x 4° scale can be interpreted (Fig. 7c). These anomalies
233 may be related with the occurrence of broad volcanism near the Sheba Ridge (d'Acremont et al.,
234 2010; Leroy et al. 2013). On the western margin of Yemen, around the city of Aden, two high
235 velocity anomalies are visible (8.2 to 8.4 km/s). These anomalies are consistent with the teleseismic
236 tomography findings of Korostelev et al. (2013) showing high velocity anomalies of about 4 % at
237 depths of 45 km and 70 km along the western margin of Yemen. Drawing on insights from receiver
238 functions analysis (Ahmed et al., 2013b), which show spatial coincidence between regions of
239 overthickened crust with a high Vp/Vs ratio and thick basalt flows (Seaward Dipping Reflectors -
240 SDRs) suggestive of underplated ultra-mafic bodies under the crust of the Red Sea and Aden
241 margins, we interpret our low velocity anomalies as underplated magmatic material. We find high
242 velocity anomalies of about 1.2 to 3.7 % relative to the mean mantle velocity beneath most of the
243 plateaus and rifted margins, with the exception of locales of Holocene to Recent volcanism. High
244 velocities are generally explained by a stable, cold and/or thick lithospheric mantle (e.g. Calvert et
245 al., 2000; Al-Lazki et al., 2004; Hearn et al., 2004; Pei et al., 2007). In this area, the rifting phase
246 terminated about 16 Ma (Davison et al. 1994; Leroy et al. 2012) and as a result the lithosphere has
247 cooled and become more stable than the area around. There is also a contrast in the crustal thickness
248 between these two areas induced by the rifting episode of the Red Sea 34 Ma (Davison et al. 1994;
249 Leroy et al. 2012). Indeed, the crustal thickness varies from 35 +/- 2 km under the high Plateaus to
250 20 +/- 3 km under the Tihama plain as found by computation of receivers functions (Ahmed et al.,

2013b).

Deep anomalies on the Eastern Oman and Gulf of Aden

The tomographic image of the DLM shows a spatial distribution of low velocity anomalies that is distinctly different from that of the SLM. In the eastern part of the gulf, imaging of the DLM between the Sheba Ridge and the Oman coast indicates a high velocity anomaly, while velocity of the mantle between the Sheba Ridge and Socotra Island is low (7.8 km/s). This low velocity in the DLM south of the ridge is consistent with the findings of Leroy et al. (2010) and d'Acremont et al. (2010) who measured significant variation of the electric resistivity beneath the oceanic crust on either side of the Sheba Ridge. Electrical resistivity of mantle to the south of the Sheba Ridge is low, indicating the presence of hot material related to an off-axis melting anomaly. To the north of the Sheba Ridge, electrical resistivity is higher and consistent with colder mantle temperatures.

A low velocity anomaly within the DLM beneath southern Oman is consistent with Basuyau et al. (2010) who imaged two low velocity anomalies in the DLM (between 60 and 200 km depth) beneath the Omani margin aligned with the Alula-Fartak and Socotra-Hadbeen Fracture Zones. The magnitude of these anomalies is consistent with the presence of partial melting (3–6 per cent). They interpret these anomalies as melt products migrating from the Sheba Ridge, as a result of upwelling Afar plume material migrating eastward along the lithosphere-asthenosphere boundary below thinned lithosphere at the ridge. The presence of a single larger low velocity anomaly (7.8 km/s) at depth in this area is suggested by our study and may indicate a broader deep zone of melting accumulation. The 5% reduction in Pn velocity relative to the mean DLM velocity could be interpreted as the presence of 1.4% melt in the DLM (Stork et al., 2013).

Plume-ridge interaction model: material channeled along the Gulf of Aden ?

Many studies have attempted to understand the influence of the Afar plume on surrounding regions and its interactions with the East-African, Red Sea and Gulf of Aden rifts (e.g. Hansen et al., 2006; Park et al., 2008; Lucazeau et al., 2009; Leroy et al., 2010; Albers and Christensen, 2001). As in

previous studies, the Pn tomographic image of the SLM shows a low velocity anomaly (7.7 km/s) beneath the Afar region (Stork et al., 2013). This is low in comparison with the global mean Pn velocity, and with other rifts and ridges which have similar extension rates (Keir et al., 2013).

The resolution of our study does not permit us to image the DLM beneath the Afar region. Our image of the shallow upper mantle beneath Afar shows a low velocity anomaly (7.9 km/s) that extends southwestward, northward and along the Aden Ridge. These zones of low velocity coincide with active volcanism and are therefore likely to be the result of melt production beneath thinned lithosphere, or partial melt within the mantle lithosphere beneath the three rift arms of the Afar triple junction. Partial melt may migrate beneath the Lithosphere-Asthenosphere boundary by channelized flow. The model proposed by Leroy et al. (2010) that calls for channeling of mantle material along the Aden Ridge implies that the Afar plume influence may extend toward the eastern Gulf of Aden. The findings of Chang and Van der Lee (2011) agree with this model for the western part of the gulf. Our SLM image of low velocity anomalies that extend from Afar toward the Sheba Ridge is consistent with channeling of plume material beneath the western Gulf of Aden. These low velocity anomalies may also be explained by small-scale convection in the mantle due to temperature gradients and/or the difference in thickness of continent and ocean lithospheres in the deep margins of the gulf (Lucazeau et al., 2008). Small-scale convection would require low velocity anomalies to be found along the entire length of the ocean-continent transition zone (OCT, Fig. 8) from east to west. Although low velocity anomalies are imaged along the OCT in the eastern gulf (southern Oman and northern Socotra Island), they do not seem to be imaged continuously between the Shukra El Sheik (SSFZ) and the Alula Fartak (AFFZ) Fracture Zones. We therefore suggest that small-scale convection may not be the only active process.

Our Pn tomography images lend credence to the plume-ridge interaction model, an interpretation also favored by the physical and rheological characteristics of the region. The Gulf of Aden is a slow-spreading (20 mm/yr.) narrow oceanic basin segmented by numerous transform faults (Fig. 8)

(Leroy et al., 2010; 2012). It has been suggested that transform faults form rheological barriers to plume dispersion along ridge axis (Georgen et al., 2003). Our results indicate this may occur in several locations in the Gulf of Aden: in the central Gulf of Aden, the Kanshar Irqah and the Xiis Mukalla fractures zones (Fig. 8). The low velocity anomaly extends northward between the latter two fracture zones, and appears to terminate at the southern coast of Yemen beneath a volcanic structure. The Bosaso Masila Fracture Zone directly aligned with an active volcano located on the southern coast of Yemen (Fig. 8) may act as a rheological barrier channeling the flow of mantle material towards the region of active volcanism to the north.

CONCLUSION

We conducted a Pn tomography study in order to image the lithospheric mantle of the Gulf of Aden from the Afar triple junction in the west to the Owen Fracture Zone in the east. We find low velocity anomalies (~7.7 km/s) in the SLM beneath Sana'a, Aden, and in the Afar region that are immediately associated with active volcanism. Low velocity anomalies imaged along the Aden and Sheba Ridges could support plume-ridge interaction model proposed by Leroy et al. (2010) in which plume material is channeled away from Afar beneath the ridges. In addition we identify low velocities along the southern coast of Yemen in regions of Holocene to Recent volcanism, and also along the nearby Kanshar Irqah and Xiis Mukalla Fractures Zones. These observations suggest that transform fault/fracture zones act as rheological barriers in some cases, diverting flow towards site of active volcanism away from the ridge. A shallow broad low velocity anomaly (7.7 km/s) is imaged in the north of Socotra island and could be related to the occurrence of broad volcanism near the Sheba Ridge. Shallow high velocity anomalies (8.4 km/s) are also imaged to the west of Sana'a and around the city of Aden. These anomalies could be related to underplating of high velocity magmatic material under the crust of the Red Sea and Aden margins. A deep low velocity anomaly is observed to the south of the Sheba Ridge (7.6 km/s, 54°E) which could be related to an off-axis melting anomaly. Finally, a deep low velocity anomaly (~7.6 km/s) is visible in Oman,

suggesting the presence of a large deep zone of partial melting accumulation and a presence of 1.4 per cent of melt.

ACKNOWLEDGEMENTS

This project was funded by the French agencies: ANR-07-BLAN-0135 YOCMAL, ANR-NT09-48546 Rift2Ridge, CNRS-INSU-PICS Yemen and Oman, and Actions Marges program. We also benefitted from the Afar Rift Consortium and SEIS-UK facility funded by the UK NERC. The global data we use are from IRIS-PASSCAL. We deeply thank Dr Issa-Al Hussein (EMC, Sultan Qaboos University, Oman) and Dr Ismael Al Ganad (Geological Survey, GSMRB, Yemen) for their support and Heather Sloan for discussion about the paper.

REFERENCES CITED

Abstract

Ahmed, A., Doubre, C., Leroy, S., Perrot, J., Audin, L., Rolandone, F., Keir, D., Al-Ganad, I., Sholan, J., Khanbari, K., Mohamed, K., Vergne, J., Jacques, E., and Nercessian, A., 2013a, Seismic constraints on a large dyking event and initiation of a transform fault zone in Western Gulf of Aden, EGU General Assembly 2013, Austria, Vienna, id. EGU2013-14000.

Korostelev, F., Basuyau, C., Leroy, S., Ahmed, A., Stuart, G., Keir, D., Rolandone, F., Al-Ganad, I., and Khanbari, K., 2013, Influence of the Afar plume on the deep structure of Aden and Red Sea margins - Insight from teleseismic tomography in western Yemen, EGU General Assembly 2013, Vienna, Austria, id. EGU2013-10564.

Leroy, S., d'Acremont, E., Lucazeau, F., Poort, J., Ahmed, A., Keir, D., Stuart, G., Khanbari, K., Bellahsen, N., and Nonn, C., 2013, How does continental crust thin in a young continental margin? Insights from Oman/Socotra conjugate margins in the eastern Gulf of Aden, EGU General Assembly 2013, Austria, Vienna, id. EGU2013-7073.

Computer Program

Paige, C. C., and Saunders, M. A., 1982, LSQR: Sparse Linear Equations and Least Squares

Problems, ACM Transactions on Mathematical Software, 8(2), p. 195-209.

Journal

Ahmed, A., Tiberi, C., Leroy, S., Stuart, G., Keir, D., Sholan, J., Khanbari, K., Al-Ganad, I., and Basuyau, C., 2013b, Crustal structure of the rifted volcanic margins and uplifted plateau of Western Yemen from receiver function analysis: Geophysical Journal International, doi: 10.1093/gji/ggt072.

Albers, M., and Christensen, U. R., 2001, Channeling of plume flow beneath mid-ocean ridges: Earth and Planetary Science Letters, v. 187, no. 1, p. 207-220.

Al-Lazki, A., Sandvol, E., Seber, D., Barazangi, M., Turkelli, N., and Mohamad, R., 2004, Pn tomographic imaging of mantle lid velocity and anisotropy at the junction of the Arabian, Eurasian and African plates: Geophysical Journal International, v. 158, p. 1024-1040, doi: 10.1111/j.1365-246X.2004.02355.x.

Bannister, S. C., Ruud, B. O., and Husebye, E. S., 1991, Tomographic estimates of sub-Moho seismic velocities in Fennoscandia and structural implications: Tectonophysics, v. 189, p. 37-53.

Basuyau, C., Tiberi, C., Leroy, S., Stuart, G., Al-Lazki, A., Al-Toubi, K., and Ebinger, C., 2010, Evidence of partial melting beneath a continental margin: case of Dhofar, in the Northeast Gulf of Aden (Sultanate of Oman): Geophysical Journal International, v. 180, p. 520-534, doi: 10.1111/j.1365- 246X.2009.04438.x.

Beghoul, N., Barazangi, M., and Isacks, B. L., 1993, Lithospheric structure of Tibet and western North America; mechanisms of uplift and a comparative study: Journal of Geophysical Research, vol. 98, p. 1997-2016.

Bellahsen, N., Faccenna, C., Funiciello, F., Daniel, J. M., and Jolivet, L., 2003, Why did Arabia separate from Africa? Insights from 3-D laboratory experiments: Earth and Planetary Science Letters, v. 216, p. 365-381.

376 Calvert, A., Sandvol, E., Sebert, D., Barazangi, M., Vidal, F., Alguacil, G., and Jabour, N., 2000,
377 Propagation of regional seismic phases (Lg and Sn) and Pn velocity structure along the
378 Africa-Iberia plate boundary zone: tectonic implications: Geophysical Journal International,
379 v. 142, p. 384-408.
380 Chang, S.-J., and Van der Lee, S., 2011, Mantle plumes and associated flow beneath Arabia and
381 East Africa: Earth and Planetary Science Letters, v. 302, p. 448-454.
382 D'Acremont, E., Leroy, S., Maia, M., Gente, P., and Autin, J., 2010, Volcanism, jump and
383 propagation on the Sheba ridge, eastern Gulf of Aden: segmentation evolution and
384 implications for oceanic accretion processes, Geophysical Journal International, v. 180, p.
385 535-551, doi: 10.1111/j.1365- 246X.2009.04448.x.
386 Davison, I. A. N., Al-Kadasi, M., Al-Khirbash, S., Al-Subbary, A. K., Baker, J., Blakey, S., Bosence,
387 D., Dart, C., Heaton, R., McClay, K., Menzies, M., Nichols, G., Owen, L., and Yelland, A.,
388 1994, Geological evolution of the southeastern Red Sea Rift margin, Republic of Yemen:
389 Geological Society of America Bulletin, v. 106, no. 11, p. 1474-1493.
390 Debayle, E., Lévêque, J.-J., and Cara, M., 2001, Seismic evidence for a deeply rooted low-velocity
391 anomaly in the upper mantle beneath the northeastern Afro/Arabian continent: Earth and
392 Planetary Science Letters, v. 193, no. 423-436.
393 Dunn, R. A., Toomey, D. R., Detrick, R. S., and Wilcock, W. S. D., 2001, Continuous Mantle Melt
394 Supply Beneath an Overlapping Spreading Center on the East Pacific Rise: Science, v. 291,
395 no. 1955, doi: 10.1126/science.1057683.
396 Ebinger, C. J., Keir, D., Ayele, A., Calais, E., Wright, T. J., Belachew, M., and Buck, W. R., 2008,
397 Capturing magma intrusion and faulting processes during continental rupture: seismicity of
398 the Dabbahu (Afar) rift: Geophysical Journal International, v. 174, no. 3, p. 1138-1152.
399 Ebinger, C. J., Ayele, A., Keir, D., Rowland, J., Yirgu, G., Wright, T., Belachew, M., and Hamling,
400 I., 2010, Length and Timescales of Rift Faulting and Magma Intrusion: The Afar Rifting

401 Cycle from 2005 to Present: Annual Review of Earth and Planetary Sciences, doi:
402 10.1146/annurev-earth-040809-152333.
403 Ebinger, C. J., van Wijk, J., and Keir, D., 2013, The time scales of continental rifting: implications
404 for global processes: Geological Society of America Special Papers, v. 500, p. 371-396.
405 Georgen, J. E., and Lin, J., 2003, Plume-transform interactions at ultra-slow spreading ridges:
406 Implications for the Southwest Indian Ridge: Geochemistry Geophysics Geosystems, v. 4,
407 no. 9, doi: 10.1029/2003GC000542.
408 Grandin, R., Jacques, E., Nercessian, A., Ayele, A., Doubre, C., Socquet, A., and King, G. C. P.,
409 2011, Seismicity during lateral dike propagation: Insights from new data in the recent Manda
410 Hararo–Dabbahu rifting episode (Afar, Ethiopia): Geochemistry, Geophysics, Geosystems,
411 v. 12, no. 4.
412 Hansen, S., Schwartz, S., Al-Amri, A., and Rodgers, A., 2006, Combined plate motion and density-
413 driven flow in the asthenosphere beneath Saudi Arabia: Evidence from shear-wave splitting
414 and seismic anisotropy: Geology, v. 34, no. 10, p. 869-872, doi: 10.1130/G22713.1.
415 Hearn, T. M., and Ni, J. F., 1994, Pn velocities beneath continental collision zones: the Turkish-
416 Iranian Plateau: Geophysical Journal International, v. 117, p. 273-283.
417 Hearn, T. M., 1996, Anisotropic Pn tomography in the western United States: Journal of
418 Geophysical Research, v. 101, no. B4, p. 8403-8414.
419 Hearn, T. M., Wang, S., Ni, J. F., Xu, Z., Yu, Y., and Zhang X., 2004, Uppermost mantle velocities
420 beneath China and surrounding regions: Journal of Geophysical Research, v. 109, no.
421 B11301, doi: 10.1029/2003JB002874.
422 Hébert, H., Deplus, C., Huchon, P., Khanbari, K., and Audin L., 2001, Lithospheric structure of a
423 nascent spreading ridge inferred from gravity data: The western Gulf of Aden: Journal of
424 Geophysical Research, v. 106, no. B11, p. 26-345.
425 Keir, D., Bastow, I. D., Pagli, C., and Ayele, A., 2011, The magma-assisted removal of Arabia in

426 Afar: Evidence from dike injection In the Ethiopian rift captured using InSAR and
427 seismicity: Tectonics, v. 30, no. TC2008, doi: 10.1029/2010TC002785.
428 Keir, D., Bastow, I. D., Pagli, C., and Chambers, E. L., 2013, The development of extension and
429 magmatism in the Red Sea rift of Afar: Tectonophysics, v. 607, p. 98-114, doi:
430 10.1016/j.tecto.2012.10.015.
431 Leroy, S., d'Acremont, E., Tiberi, C., Basuyau, C., Autin, J., Lucazeau, F., and Sloan, H., 2010,
432 Recent off-axis volcanism in the eastern Gulf of Aden: Implications for plume-ridge
433 interaction: Earth and Planetary Science Letters, v. 293, p. 140-153.
434 Leroy, S., Razin, P., Autin, J., Bache, F., d'Acremont, E., Watremez, L., Robinet, J., Baurion, C.,
435 Denèle, Y., Bellahsen, N., Lucazeau, F., Rolandone, F., Rouzo, S., Serra Kiel, J., Robin, C.,
436 Guillocheau, F., Tiberi, C., Basuyau, C., Beslier, M.-O., Ebinger, C., Stuart, G., Ahmed, A.,
437 Khanbari, K., Al-Ganad, I., de Clarence, P., Unternehr, P., Al-Toubi, K., and Al-Lazki A.,
438 2012, From rifting to oceanic spreading in the Gulf of Aden: a synthesis: Arabian Journal of
439 Geosciences, v. 2, no. 2, doi: 10.1007/s12517-011-0475-4.
440 Lucazeau, F., Leroy, S., Bonneville, A., Goutorbe, B., Rolandone, F., d'Acremont, E., Watremez, L.,
441 Düsünur, D., Tuchais, P., Huchon, P., Bellahsen, N., and Al-Toubi, K., 2008, Persistent
442 thermal activity at the Eastern Gulf of Aden after continental break-up: Nature Geosciences,
443 v. 1, p. 854–858, doi: 810.1038/ngeo1359.
444 Lucazeau, F., Leroy, S., Autin, J., Bonneville, A., Goutorbe, B., Watremez, L., d'Acremont, E.,
445 Düsünur, D., Rolandone, F., Huchon, P., Bellahsen, N., and Tuchais, P., 2009, Post-rift
446 volcanism and high heat-flow at the ocean-continent transition of the eastern Gulf of Aden:
447 Terra Nova, v. 21, p. 285-292, doi: 10.1111/j.1365-3121.2009.00883.x.
448 Nobile, A., Pagli, C., Keir, D., Wright, T. J., Ayele, A., Ruch, J., and Acocella, V., 2012, Dike-fault
449 interaction during the 2004 Dallol intrusion at the northern edge of the Erta Ale Ridge (Afar,
450 Ethiopia): Geophysical Research Letters, v. 39, no. L19305, doi: 10.1029/2012GL053152.

Park, Y., Nyblade, A. A., Rodgers, J. and Al-Amri, A., 2007, Upper mantle structure beneath the Arabian Peninsula and northern Red Sea from teleseismic body wave tomography: Implications for the origin of Cenozoic uplift and volcanism in the Arabian Shield: Geochemistry Geophysics Geosystems, v. 8, no. 6, doi: 10.1029/2006GC001566.

Park, Y., Nyblade, A. A., Rodgers, J., and Al-Amri, A., 2008, S wave velocity structure of the Arabian Shield upper mantle from Rayleigh wave tomography: Geochemistry Geophysics Geosystems, v. 9, no. 7, doi: 10.1029/2007GC001895.

Pei, S., Zhao, J., Sun, Y., Xu, Z., Wang, S., Liu, H., Rowe, C. A., Toksöz, M. N., and Gao, X., 2007, Upper mantle seismic velocities and anisotropy in China determined through Pn and Sn tomography: Journal of Geophysical Research, v. 112, no. B05312, doi: 10.1029/2006JB004409.

Perry, H. K. C., Jaupart, C., Mareschal, J.-C., and Shapiro, N. M., 2006, Upper mantle velocity-temperature conversion and composition determined from seismic refraction and heat flow: Journal of Geophysical Research, v. 111, no. B07301, doi: 10.1029/2005JB003921.

Phillips, W. S., Begnaud, M. L., Rowe, C. A., Steck, L. K., Myers, S. C., Pasyanos, M. E., and Ballard, S., 2007, Accounting for lateral variations of the upper mantle gradient in Pn tomography studies: Geophysical Research Letters, v. 34, no. L14312, doi: 10.1029/2007GL029338.

Rolandone, F., Lucazeau, F., Leroy, S., Mareschal, J.-C., Jorant, R., Goutorbe, B., and Bouquerel, H., 2013, New heat flow measurements in Oman and the thermal state of the Arabian shield and platform: Tectonophysics, v. 589, p. 77-89, doi: 10.1016/j.tecto.2012.12.034.

Shuler, A., and Nettles, M., 2012, Earthquake source parameters for the 2010 western Gulf of Aden rifting episode: Geophysical Journal International, doi: 10.1111/j.1365-246X.2012.05529.x.

Stork, A. L., Stuart, G. W., Henderson, C. M., Keir, D., and Hammond, J. O. S., 2013, Uppermost mantle (Pn) velocity model for the Afar region, Ethiopia: An insight into rifting process:

Geophysical Journal International, v. 193, p. 321-328, doi: 10.1093/gji/ggs106.

Wright, T. J., Ebinger, C., Biggs, J., Ayele, A., Yirgu, G., Keir, D., and Stork, A. L., 2006, Magma-maintained rift segmentation at continental rupture in the 2005 Afar dyking episode: Nature, v. 442, p. 291-294, doi: 10.1038/nature04978.

Web Site

International Seismological Centre, On-line Bulletin, Internatl. Seis. Cent., Thatcham, United Kingdom:
http://www.isc.ac.uk (2011).

FIGURES

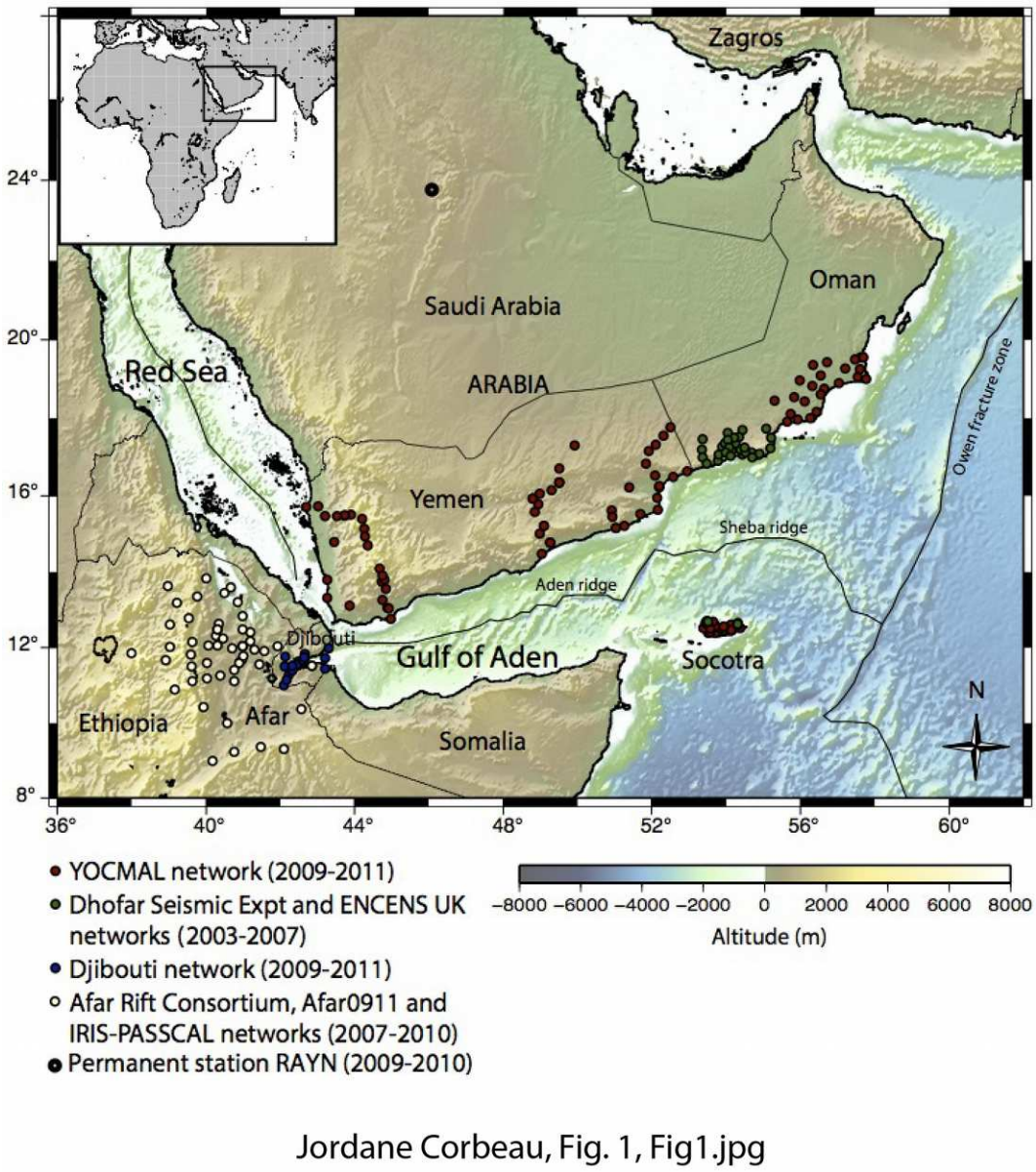

Jordane Corbeau, Fig. 1, Fig1.jpg

Figure 1. Topographic and bathymetric map of the study area. The locations of the seismic stations from different temporary networks used in this study are indicated by circles.

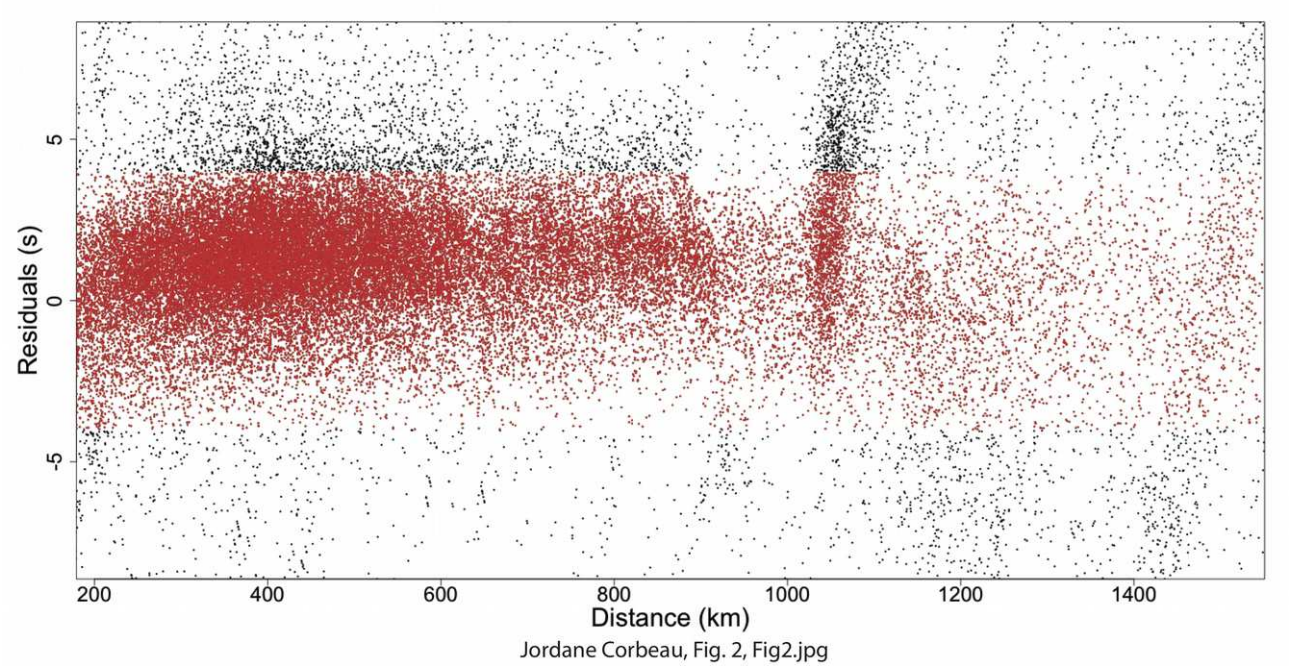

Figure 2. Plot of the travel times from the total data set relative to an initial uppermost mantle velocity of 8.16 km/s. The vertical trend of the residuals around 1000 km could be due to mislocated events. We use strict criteria (see text) to select the data and furthermore we only use the travel times with residuals less or equal to 4 s in the Pn tomography inversion as shown in red in the figure.

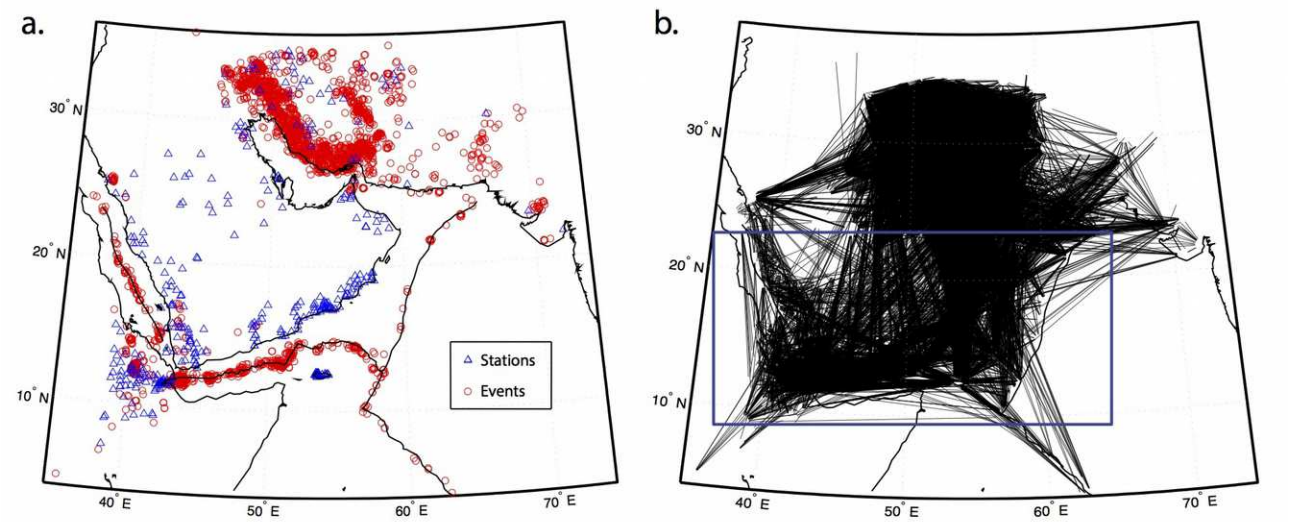

Jordane Corbeau, Fig. 3, Fig3.jpg

Figure 3. A: Map of stations (blue triangles, temporary networks and catalogues) and seismic events (red circles) used for the inversion. A total of 3,778 events and 352 stations are used. B: Pn rays used for the inversion. A total of 52,947 rays were selected. Only the results of the blue rectangle area are discussed in this study.

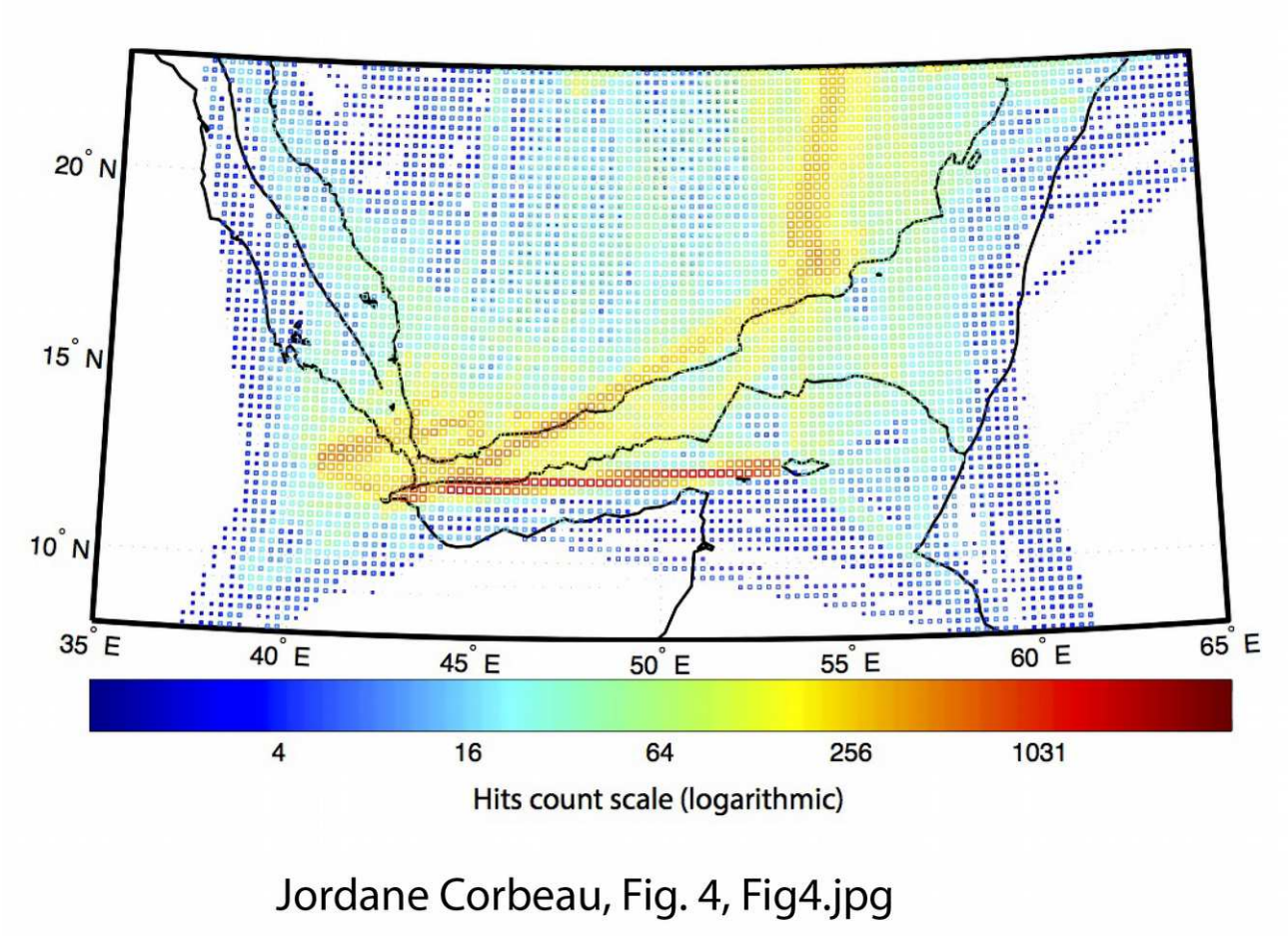

Figure 4. Number of rays traveling in each cell of the 2D grid model. Ray coverage is dense near the Afar triple junction, the north coast of the Gulf of Aden, and between Afar and the Socotra Island.

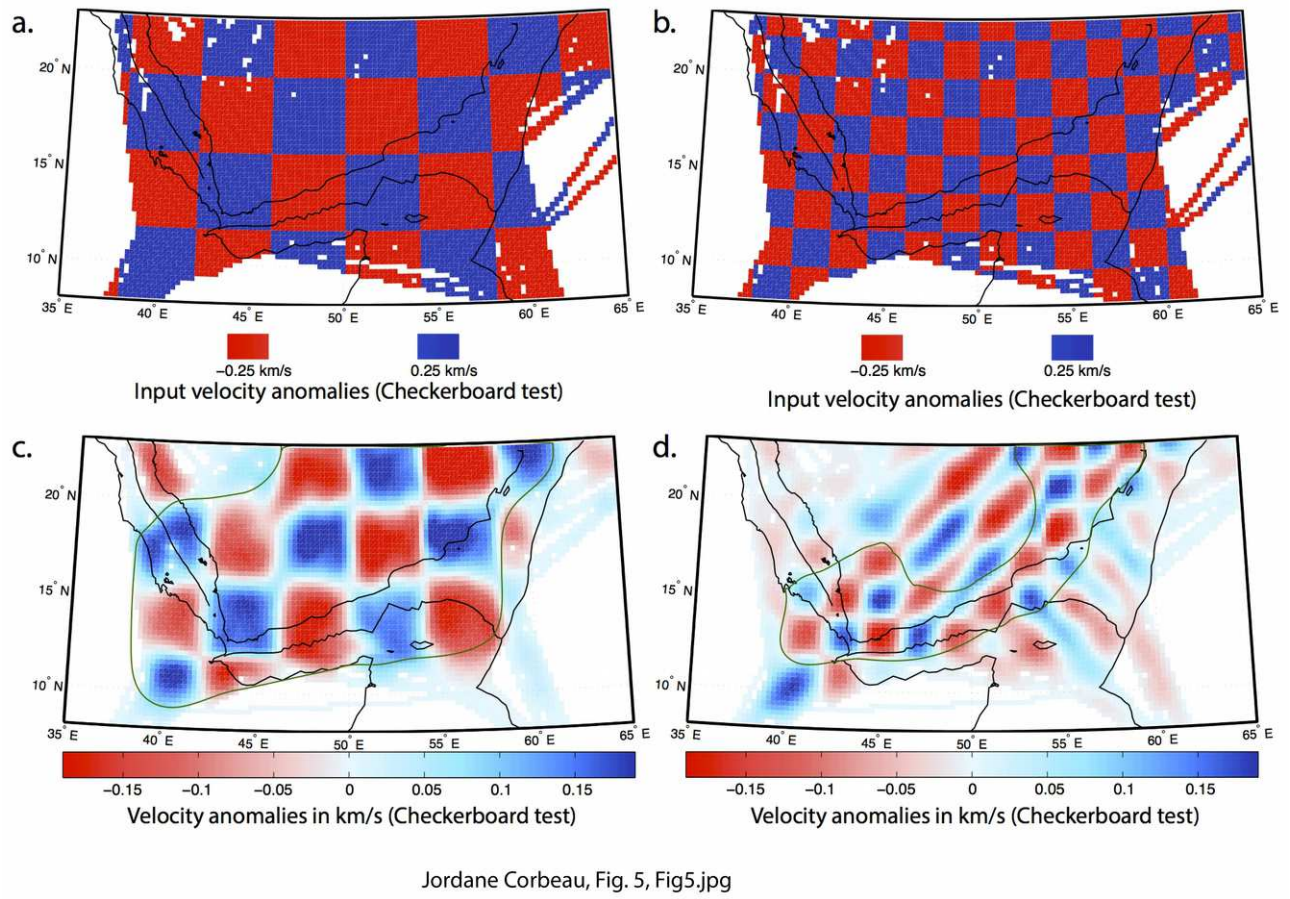

Figure 5. Pn velocity checkerboard tests. A: Input checkerboard test (4° by 4°). B: Input checkerboard test (2° by 2°). C: 4° by 4° checkerboard test resolved, the green line delimits the resolution area. D: 2° by 2° checkerboard test resolved, the green line delimits the resolution area. Synthetic data are generated with 0.25 km/s isotropic velocity perturbations and a 1s random Gaussian noise to simulate Pn picking errors. In the Afar region and along the north coast of the Gulf of Aden, features as small as 2° can be resolved, while in the rest of the study area, the resolution limit is 4° or larger.

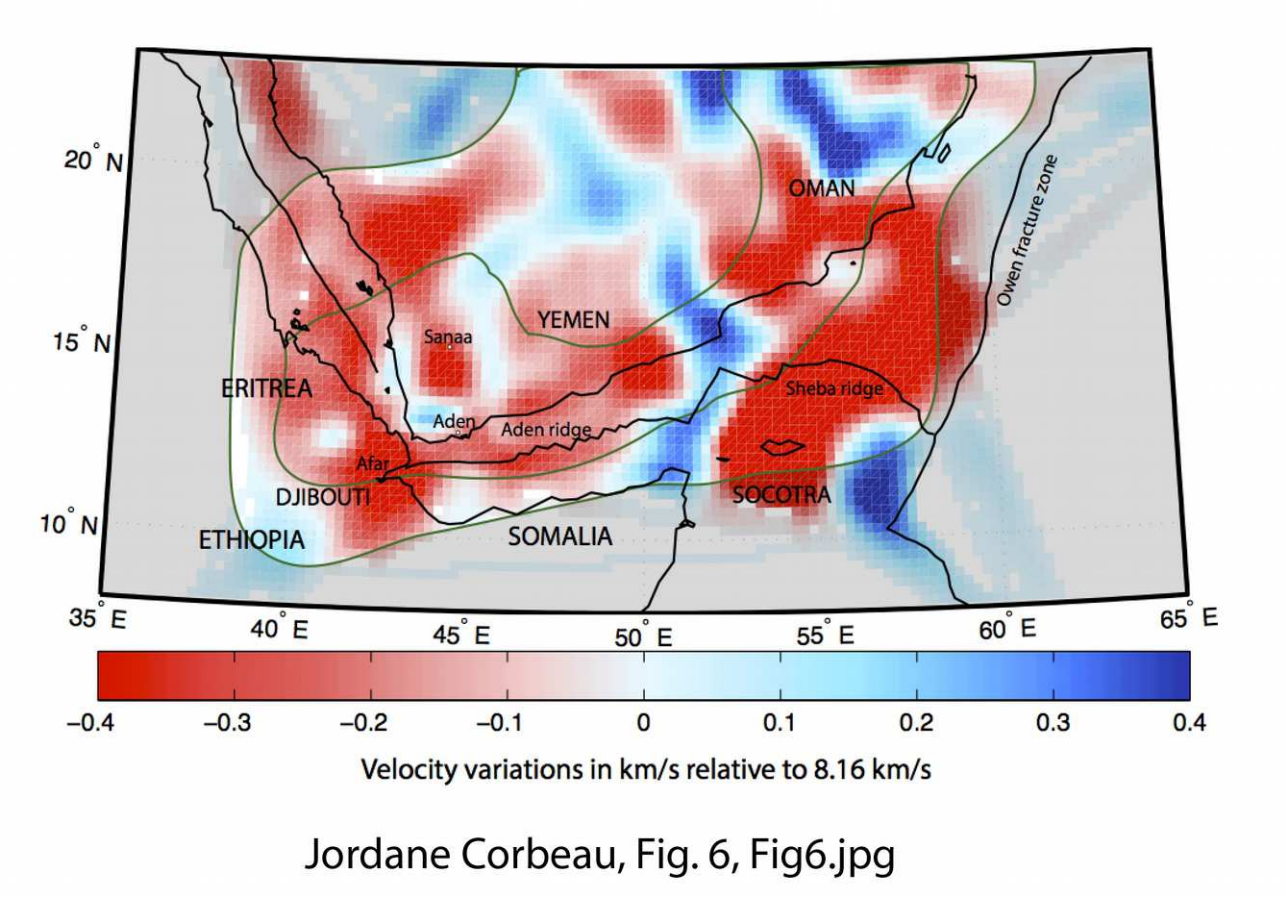

Figure 6. Variation of mantle Pn velocity in km/s relative to the mean velocity of 8.1 km/s. This inversion used ray paths from 1.8° to 16°. The cell size is 0.25° by 0.25°. The surrounding green line delimits the area of 4° resolution and the inside green line the 2° resolution area.

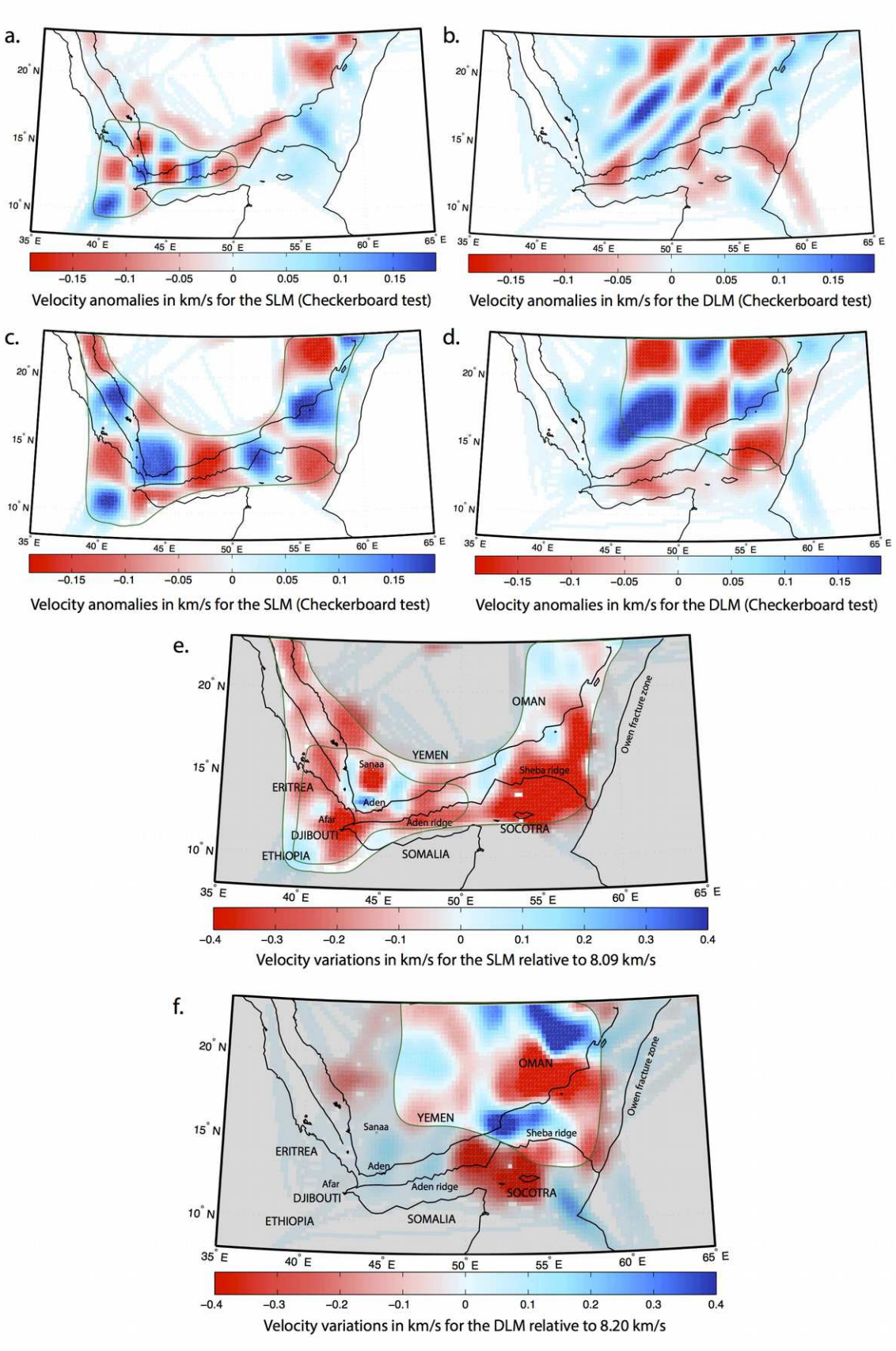

Jordane Corbeau, Fig. 7, Fig7.jpg

Figure 7. Checkerboard tests for short ray path inversion (1.8° to 9.5°) and long ray path inversion (9.5° to 16°), and variation of Pn velocity for the Shallow Lithospheric Mantle (SLM) and the Deeper Lithospheric Mantle (DLM). A: 2° by 2° checkerboard test for the SLM. B: 2° by 2° checkerboard test for the DLM. C: 4° by 4° checkerboard test for the SLM. D: 4° by 4° checkerboard test for the DLM. The green lines delimit the different resolution areas. E: Variation of SLM Pn velocity in km/s relative to the mean velocity of 8.09 km/s. The surrounding green line delimits the area of 4° resolution and the inside green line the 2° resolution area. F: Variation of DLM Pn velocity in km/s relative to the mean velocity of 8.20 km/s. Note that the scale is different between Figure 7e and 7f due to a different mean velocity calculated by the model. The green line delimits the 4° resolution area.

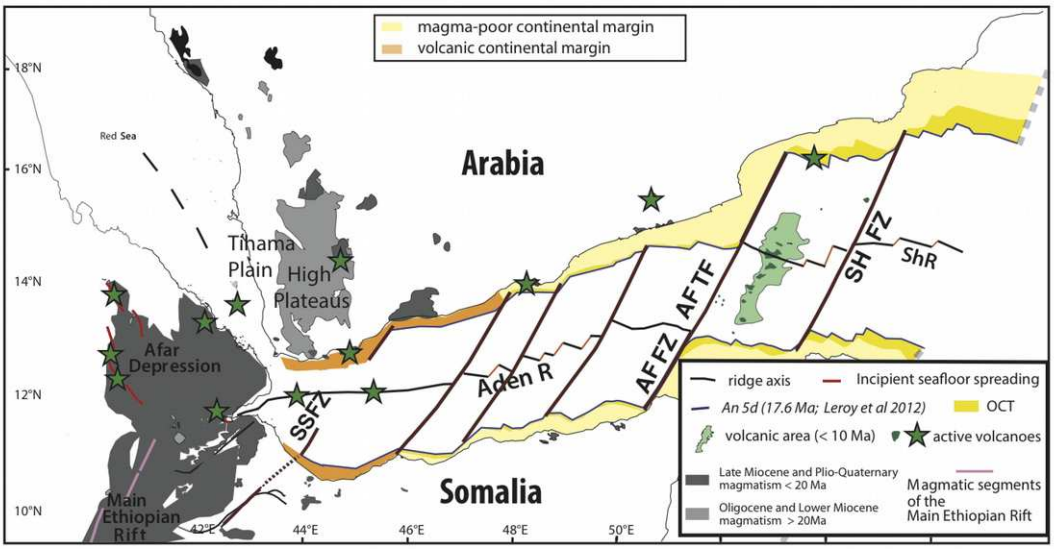

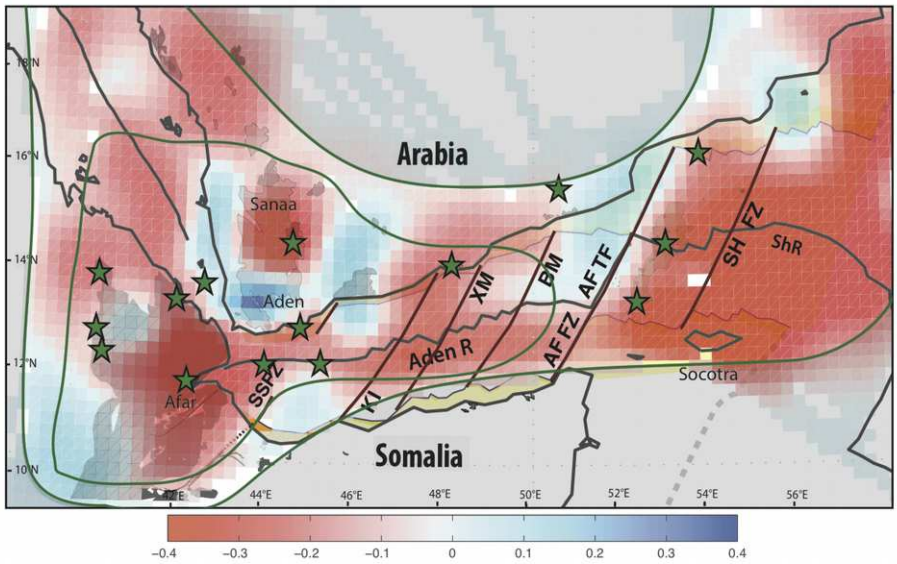

SHALLOW LITHOSPHERIC MANTLE

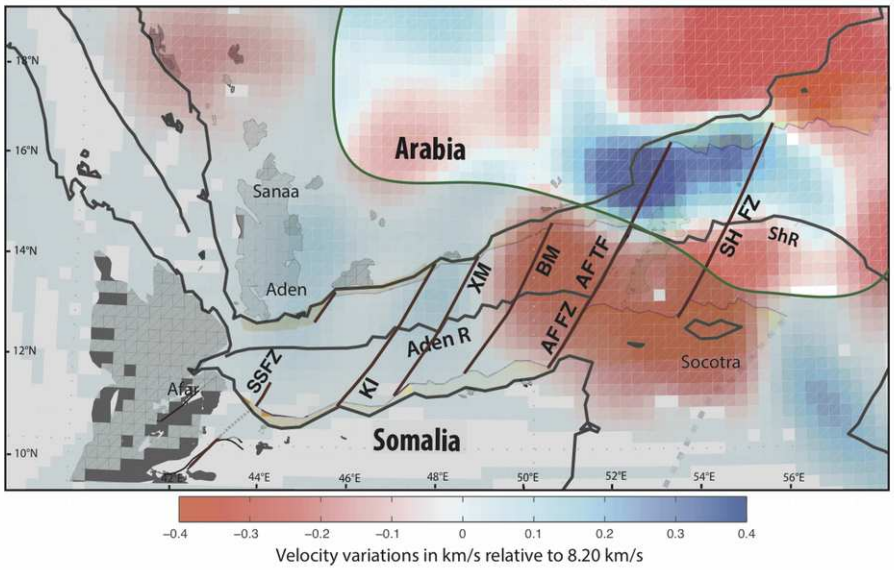

DEEPER LITHOSPHERIC MANTLE

Jordane Corbeau, Fig. 8, Fig8.jpg

Figure 8. Superposition of the velocity images of the SLM (middle) and DLM (bottom) on a map of the magmatic and volcanic activity (top, modified from Ebinger et al., 2008 and Leroy et al., 2010; 2012). Aden R = Aden ridge, ShR = Sheba ridge, SSFZ = Shukra el Sheik Fracture Zone, KI = Kanshar-Irqah, XM = Xiis-Mukalla, BM = Bosaso-Masila, AFFZ = Alula-Fartak Fault Zone, AFTZ = Alula-Fartak Transform Zone, SHFZ = Socotra Hadbeen Fault Zone, OCT = Ocean-Continent Transition. The surrounding green line delimit the area of 4° resolution and the inside green line the 2° resolution area.

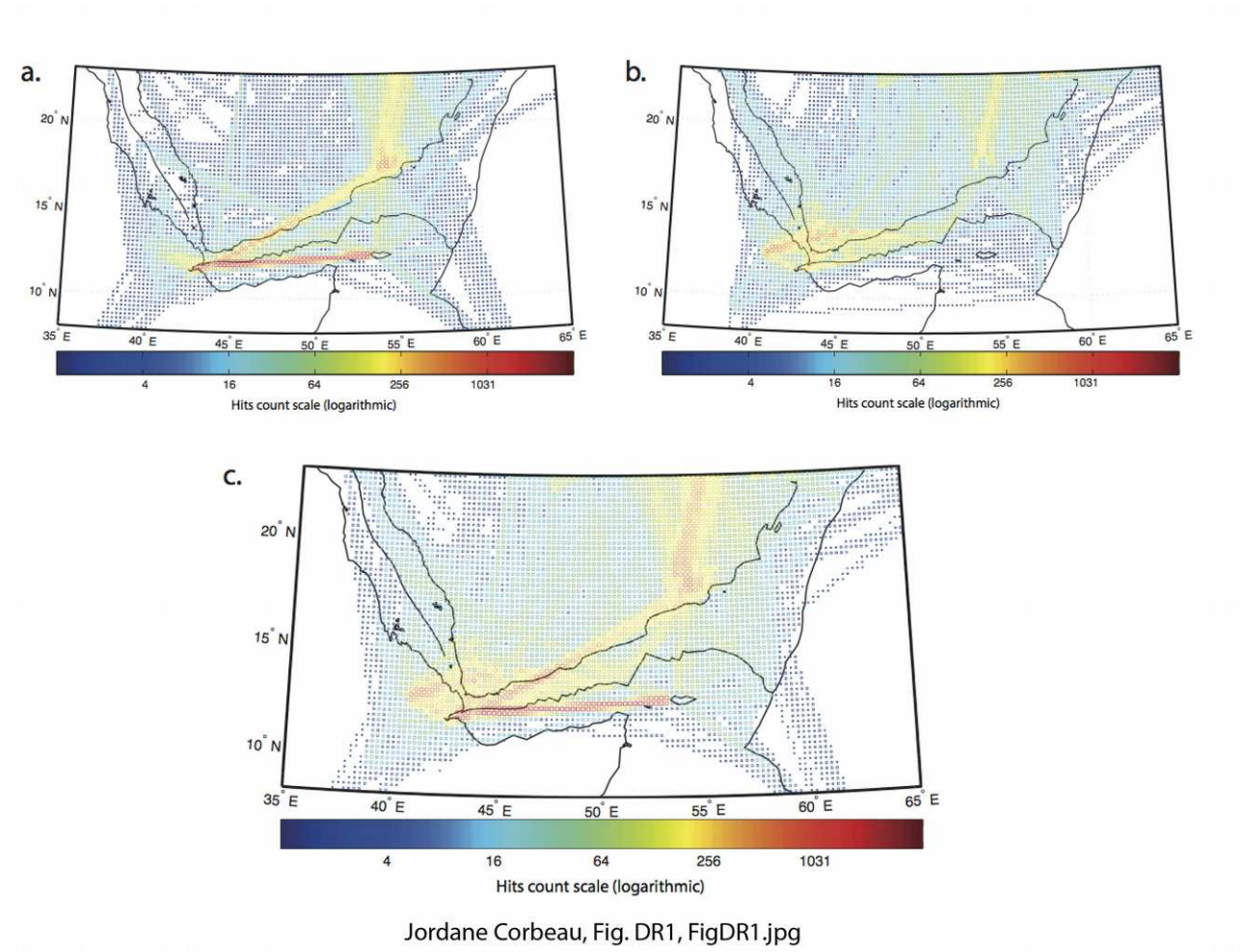

Figure DR1. Number of rays traveling in each cell of the 2D grid model. A: Ray density for the temporary seismic network data set. B: Ray density for the ISC catalogue data set. C: Ray density for the total data set used in this study, combining the ISC catalogue and the temporary seismic network data sets. The combined data set has a higher density of rays in the Gulf of Aden and Afar

539 areas.

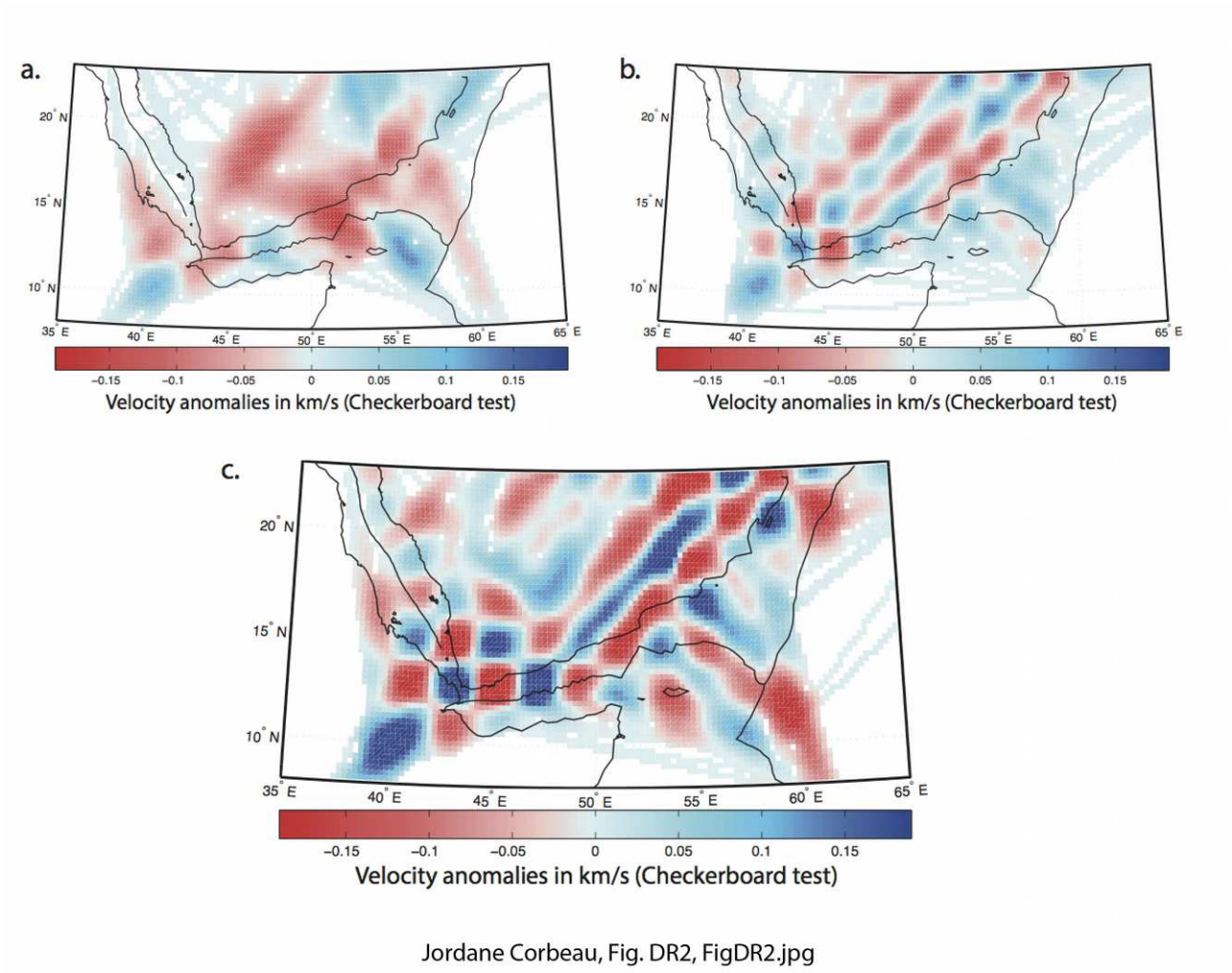

541 Figure DR2. 2° by 2° checkerboard test resolved. Synthetic data are generated with 0.25 km/s
542 isotropic velocity perturbations and a 1s random Gaussian noise to simulate Pn identification errors.
543 A: Checkerboard test for the temporary seismic network data set. B: Checkerboard test for the ISC
544 catalogue data set. C: Checkerboard test for the total data set used in this study, combining the ISC
545 catalogue and the temporary seismic network data sets. The checkerboard test for the combined data
546 set shows better 2° by 2° resolution in the southwest of Yemen, in Afar and along the Gulf of Aden
547 north coast.